Numerical study of the influences of pressure confinement on high-speed impact tests of dynamic material properties of concrete

Jian Cui, Hong Hao* and Yanchao Shi

Tianjin University and Curtin University Joint Research Centre of Structural Monitoring and Protection, School of Civil Engineering, Tianjin University, China

School of Civil and Mechanical Engineering, Curtin University, Australia

Abstract: The strain rate effect of concrete material under multi-axial stress states in most of the current material models is based on the uniaxial impact test results because carrying out multi-axial dynamic impact tests is extremely hard. However, the uniaxial test data might not reflect the true behavior of concrete under multi-axial stress states. Modified Split-Hopkinson Pressure Bar (SHPB) system with a pressure vessel filled with pressurized fluid or air is commonly used to test the concrete dynamic properties under confining pressures. Although such tests give concrete material properties under multi-axial stress states, as will be demonstrated in this study, they do not lead to accurate results because the confining pressure under impact tests changes when specimen deforms. Unfortunately there is no reliable apparatus yet to perform impact tests on specimens with a controllable confining pressure. In this study, a mesoscale concrete model with consideration of randomly distributed aggregates is developed to study the strain rate effect on concrete under confining pressures. The results show that the strain rate sensitivity of concrete decreases with the increment of the confining pressure, indicating the strain rate effect of concrete under multi-axial stress states is less prominent as compared to that under uniaxial stress state. Using the uniaxial impact testing

* Corresponding author: hong.hao@curtin.edu.au (H. Hao)

data overestimates the strain rate effect of concrete material under multi-axial stress states. An empirical relation is proposed in this study to model the concrete Dynamic Increase Factor (DIF) for the case with pressure confinement, which can be used to more accurately represent the DIF of concrete material under multi-axial stress states.

Keyword: Concrete constitutive model; strain rate effect; SHPB test; confining pressure; mesoscale model.

1. Introduction

Concrete structures during their service life might expose to multi-hazard loadings such as blast and impact loads. Under such dynamic loads, the stress states of concrete material are very complex owing to the complex stress wave propagations induced by blast and impact loads and inertial confinement from concrete structure mass to resist fast dynamic deformations. The dynamic behavior of concrete material under multi-axial stress states is not well understood yet due to the lack of proper testing facilities for conducting multi-axial impact tests, as well as the lack of effective analysis methods to predict the dynamic performance of concrete under such conditions [1]. Most existing concrete material models adopt the uniaxial testing results for modelling the strain rate effect of concrete material properties under multi-axial stress states, such as Equation of State (EoS) and Strength Envelope [2]. Obviously strain rate effect obtained from uniaxial impact tests is not able to reliably represent the true strain rate effect on concrete material under multi-axial stress states. Although the uniaxial impact testing data on confined concrete specimen give the dynamic behavior of concrete under multi-axial stress states, it will be proved in this study that the current testing technique, i.e., the Modified Split-Hopkinson Pressure Bar (SHPB) system with a pressure vessel filled with pressurized fluid, does not give reliable results because the confinement pressure changes when specimen deforms under impact loads. However, the reliability of numerical simulations of structural responses subjected to blast and impact loads, which have been becoming more and more common in practice, depend on the accuracy of material models. Therefore accurate modelling of the dynamic material properties of concrete under multi-axial stress states are deemed necessary.

The dynamic behavior of concrete under uniaxial loadings has been extensively investigated through experimental tests and numerical simulations [3-6]. It is found that the uniaxial strength of concrete increases with the increment of strain rate. Fib model code for concrete structures 2010 [7] gives recommendations of concrete material DIF (Dynamic Increase Factor, defined as the ratio of dynamic-to-static strength) as a function of strain rate that can be used in the design and analysis. The behavior of concrete materials subjected to tri-axial static loadings have been studied by many researchers. It is found that concrete showed different performances under multi-axial stress states, and confinement greatly improves the maximum strength and the ductility of concrete [8-11]. Nevertheless, study of strain rate effect on concrete under multi-axial stress states is very limited because of the difficulties in conducting synchronized multi-axial impact tests. When strain rate is relatively low, servo hydraulic multi-axial testing system can be used to study concrete dynamic properties under certain confining pressures. Yan et al. [12] carried out a series of low strain rate tests (< 0.1 1/s) and concluded that the strength of concrete tended to be independent of the strain rate when the confining pressure was higher than its uniaxial static strength. Fujikake et al. [13] also found that the strain rate effect on concrete maximum strength under tri-axial stress states decreased with the increment of the confining stress at a strain rate range from 3.0×10^{-2} 1/s to 2.0 1/s. Owing to the difficulty in conducting the synchronized tri-axial impact tests, for high strain rate, modified SHPB test system with a pressure vessel or using steel wrapped specimens to give confining pressures is normally used to generate pseudo tri-axial dynamic loadings. Chen et al. [14] used steel wrapped specimens to study the concrete dynamic properties under passive confining pressures. It was found that the dynamic damage evolution process was delayed significantly by the confining pressure and the strength of concrete increased obviously. However, it was noted that the confining pressure was certainly increasing and uncontrollable during the dynamic tests. Xue and Hu [15] used pressurized oil to fill the pressure vessel to give confining pressures in the mortar SHPB tests and found that the strain rate effect on mortar was obvious. Marvern et al. [16] used pressurized water to provide confinements on concrete specimens in impact tests. The results showed that concrete was sensitive to strain rate within the tested confinement pressure range of 3-10 MPa. Gary and Bailly [17] used a similar device and found that the strength of concrete increased about 30% as strain rate increased from 250 1/s to 600 1/s under 5.0 MPa confining pressure. They also found that the same level of oil pressure and air pressure led to different results, which meant that the pressurized fluid influenced the test results under dynamic loadings. As will be demonstrated in this study, the confinement media affecting the testing results is because the pressurized fluid constrains the lateral deformation of the specimen under fast loading tests; and deformation of the specimen makes the confining pressure change, hence influences the testing results. Since it is hard to keep the confining pressure constant with the current testing devices in impact tests, but changing the confining pressure with the specimen deformation during the test makes the testing data unreliable, the dynamic properties and strain rate effects of concrete material under multi-axial stress states therefore cannot be necessarily accurate obtained with the current testing devices. For these reasons, most of the current concrete material models use the strain rate effect relation obtained from uniaxial stress state to represent those of tri-axial stress states [18].

On the other hand, with development of computer technologies and computational mechanics methods, numerical simulations of uniaxial high-speed impact tests of concrete specimens have been reported and yielded good results [19-21]. In other words, numerical simulation of impact tests of concrete specimens is viable. Since it is difficult to obtain reliable results through physical tests of concrete specimens under complex dynamic stress states, in the present study, numerical simulations are utilized to simulate the modified SHPB test on concrete specimens with confinement pressures. It has been widely accepted that the true DIF of concrete material is mainly caused by the different failure modes of specimens under static and dynamic loadings [21-26]. Under static loading, the cracks develop and propagate along the weak zones of the concrete. While under dynamic loading, there is not enough time for the cracks to find the weak zones inside the concrete. Therefore widely spread cracks are forced to propagate through the higher resistance zone inside the concrete specimen. To capture these phenomena, in numerical modelling heterogeneity properties of concrete need be modelled. Mesoscale concrete model can reflect the heterogeneity and anisotropy of the material [19, 20, 27]. In this study, a mesoscale concrete model with consideration of mortar matrix and randomly distributed aggregates is developed to explore the strain rate effect on concrete under confining pressures. The accuracy of the model is verified by comparing the numerical and available testing data of uniaxial impact tests. The evolutions of the cracks under low rate loading, high rate loading and axial loading with confining pressures are studied using the mesoscale concrete model. The results are compared and discussed. Discussions on the accuracy of the current SHPB test with pressure confinement on dynamic properties of concrete under multi-axial stress states, and possible improvement on concrete constitutive models are also made.

2. Influence of the confinement pressure on the modified SHPB test results

As mentioned above, the current understanding about the strain rate effect on concrete under confining pressure may not be accurate because of the difficulty in providing a constant confining pressure to the concrete specimen in dynamic tests. In this section, numerical models of the SHPB tests without or with pressure confinement vessels are developed to simulate the tests. The accuracy of the model is verified by actual SHPB testing data without confinement.

The variation of confinement pressure during the impact tests and its influences on testing data are demonstrated through numerical simulation results.

2.1 SHPB technique

Fig. 1 gives the schematic illustration of SHPB test system which consists of an incident bar and a transmitted bar with a specimen sandwiched between them. The one-dimension incident wave is produced by a strike bar impacting the incident bar and is recorded by strain gauge A. Part of the incident wave is reflected as a tensile stress wave (also recorded by strain gauge A) at the interface between the incident bar and the specimen, while another part travels through the specimen. The wave goes forth and back between the two end surfaces of specimen and makes the stress distribute uniformly in the specimen after a few reflections [28]. The compressive stress wave leaves the specimen, then propagates forward along the transmitted bar and is recorded by strain gauge B.

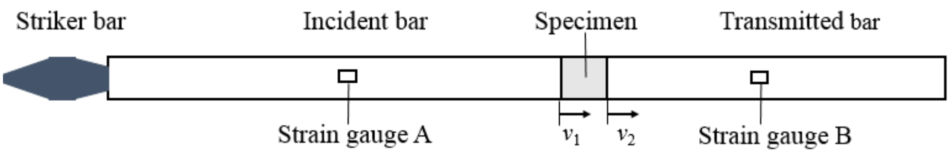

Fig. 1 SHPB test system

The compressive stress in the specimen can be deduced from the axial strain signal of strain gauge B on the transmitted bar. The compressive stress of the specimen is:

$$\sigma = \frac{A_t E \varepsilon_t}{A_s} \tag{1}$$

where A_t and A_s are the cross sectional area of the transmitted bar and specimen, respectively; E is the Young's modules of the steel bar and ε_t is the axial strain of the transmitted bar measured by strain gauge B.

The particle velocity at the end of the incident bar and transmitted bar are v_1 and v_2, respectively (as shown in **Fig. 1**). Thus the strain rate of the specimen is

$$\dot{\varepsilon} = \frac{v_1 - v_2}{l} \tag{2}$$

where l is the length of the specimen.

$$v_2 = C_B \cdot \varepsilon_t \tag{3}$$

$$v_1 = C_B \cdot (\varepsilon_i - \varepsilon_r) \tag{4}$$

where C_B is the velocity of stress wave in the steel bar, ε_i, ε_t and ε_r represent the incident strain, transmitted strain and reflected strain from the strain gauges.

The strain of specimen is

$$\varepsilon = \frac{C_B}{l} \int_0^t (\varepsilon_i - \varepsilon_r - \varepsilon_t) dt \tag{5}$$

The strain rate constantly varies throughout the SHPB test. The representative strain rate is usually determined by either of the three methods: the strain rate corresponding to the peak stress in the stress-strain curve, the average strain increasing rate before the peak stress in the stress-strain curve and the average strain rate of the entire experimental process [23]. The strain rate at the peak stress is adopted in this study.

Schematic illustration of the modified SHPB test system integrated with a pressure vessel is shown in **Fig. 2**. In this set-up, pressurized fluid is applied to the specimen through fluid pipes that are attached to a hydraulic pressure supply system, attached to the pressure vessel. A test specimen is placed between the bars, and the rubber seal is applied over the bar diameters and the specimen. The data acquisition technique of this modified SHPB is the same as that of the normal SHPB test system.

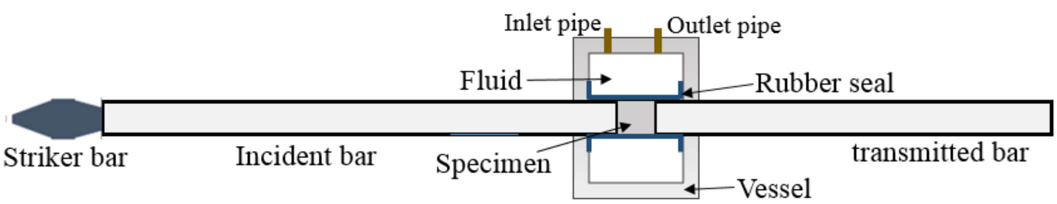

Fig. 2 Sketch of the modified SHPB test system with a pressure vessel

2.2 3D mesoscale concrete model

2.2.1 Establishment of the 3D mesoscale concrete model

In the meso-scale model, concrete specimen is assumed to be a two-phase composite material consisting of coarse aggregates and mortar matrix. A FORTRAN program is developed to generate randomly distributed aggregates and finite element meshes for the mesoscale concrete model. The size of coarse aggregates considered in the mesoscale model ranges from 3 mm to 10 mm which is assumed to follow Fuller's curve [20]. The total volume of coarse aggregates is 45% according to the mix of the concrete specimen with a compressive strength of 32.5 MPa. A cylindrical concrete specimen (the length and the diameter of specimen are both 50 mm) modelled by 1.0 mm Lagrange solid elements is considered in this study, as shown in the **Fig. 3**. Details of the development of the mesoscale model is provided in references [20, 29]. For brevity they are not repeated here.

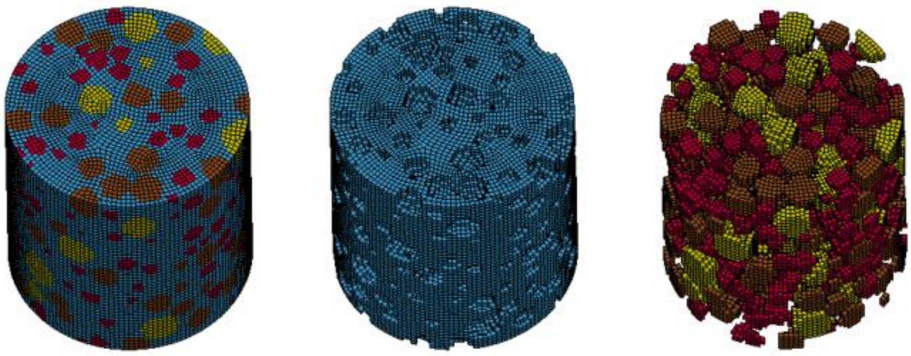

Fig. 3 Finite element grid of 3D mesoscale concrete model: (a) concrete; (b) mortar matrix; (c) coarse aggregates

K&C model [30] for concrete in LS-DYNA [31] is used to model the mortar matrix and coarse aggregates in the simulation [20]. K&C model is an elastic-plastic damage model with consideration of strain rate effect. In this model three fixed independent strength envelopes, i.e. yield, maximum and residual surfaces are defined. For hardening behavior, the loading surface is interpolated between the yield and the maximum surfaces based on a plasticity variable. For softening behavior, a similar interpolation is performed between the maximum and the residual surface. The EoS employed in LS-DYNA by the K&C model is defined using tabular input to define the relationships between volumetric strain and pressure. The automatic parameter generation for K&C model is used in the simulation and the input material parameters are listed in **Table 1**. The material DIF is set to 1.0 in the simulation in order to better observe the contributions of the mesoscale heterogeneity and inertial confinement to the dynamic strength enhancement.

Table 1 Material parameters of mortar and aggregate

Parameters	Mortar	Aggregate
Density (kg/m^3)	2100	2600
Poisson’s ratio	0.19	0.16
Strength (MPa)	30	90

2.2.2 Model validation.

(1) Low strain rate

Corresponding laboratory tests were carried out to verify the mesoscale concrete model. The specimen used in the tests was the same as described above in developing the numerical model. Before the test, the surfaces of specimens were smoothed by a polisher and coated with grease to reduce the friction between the specimen and the rigid loading platens. To investigate the possible friction constraint, the friction coefficients were measured between the greased specimen and steel surface. The average friction coefficient was found to be 0.105, which is considered in the simulation. The specimen was tested to have a 32.5 MPa uniaxial strength (strain rate is 10^{-3} 1/s) using a 500kN computer-controlled servo hydraulic pressure testing machine.

In the simulation the mesoscale concrete specimen is also sandwiched between the two rigid loading platens like that in the test. All directions of the bottom plate are restrained and the upper plate can move along the vertical direction with controlled displacement to give the specimen axial loadings as in the tests. The load transfers to the specimen by using *CONTACT_ AUTOMATIC_ SURFAE_ TO_ SURFACE command card and the friction coefficient is set to 0.105 from the measurements. The strength of specimen is simulated to be 33.4 MPa at a strain rate of 0.1 1/s which is almost the same as the static test results of 32.5 MPa, as shown in **Fig. 4**. The numerical simulation satisfactorily repeats the laboratory test when the loading rate is low. It should be noted here, the strain rate in the simulation is higher than that in the test because very low loading rate leads to extremely large computational time. In the simulation, strain rate of 0.05 1/s was also tried and it gave almost the same result as that using strain rate 0.1 1/s, implying the mesoscale concrete model is strain rate insensitive when the strain rate is lower than 0.1 1/s. This result is consistent with the conclusion based on test data that the strain rate effect of concrete compressive strength is not obvious when the strain rate is lower than 0.1 1/s [3]. Therefore strain rate 0.1 1/s is used in the simulations to represent the pseudo-static condition in the present study.

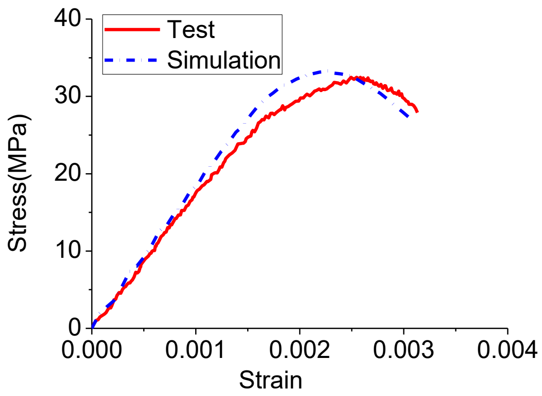

Fig. 4 Stress-strain curve of concrete under low strain rate.

(2) High strain rate

For high strain rate, numerical simulation of SHPB test with a mesoscale concrete specimen is carried out to repeat the laboratory test. In the test, the Ø75 mm steel bar has a Young's modulus of 210 GPa, density 7800 kg/m^3 and Poisson's ratio 0.28. The steel bars remain elastic in SHPB tests, therefore the isotropic elastic model (Mat_1) in LS-DYNA is used in the simulation. The material parameters of the bars used in the simulation is the same as that in the tests. *CONTACT_ AUTOMATIC_ SURFAE_ TO_ SURFACE command is used to simulate the contact between the bars and the specimen, the friction factor between the surfaces of specimen and the end surfaces of the bars is also set to 0.105. The mesh size of the elastic steel bars is 4.0 mm (cubic Lagrange solid elements) which are proven yielding reliable predictions through mesh convergence tests. The input incident stress wave is a sine wave as shown in **Fig. 5** (a), which is the same as that recorded in the test produced by a cone-shaped strike bar.

Fig. 5 compares the simulation results and the test results at strain rate about 65 1/s. It can be seen that the simulated stress histories agree reasonably well with the test data, the simulated reflected wave is slightly larger, while the simulated transmitted wave is slightly smaller than their respective counterparts recorded in the test, implying the simulated dynamic strength is smaller than the recorded strength, as shown in **Fig. 5** (b). This difference can be attributed to the no strain rate enhancement assumption in the numerical model, i.e., the DIF is defined to be 1.0 in the numerical model as described above. It is well known that a few factors contribute to the concrete strength increment in impact tests [32]. These include lateral inertial confinement [33, 34] , failure modes [22], viscosity associated to the humidity and trapped water and air in micro voids [2, 35], and strain rate effects on cement and aggregate material [36]. The mesoscale model developed in this study with unit DIF assumption captures the contributions to strength increment of concrete specimen related to the failure modes, i.e. there is not sufficient time for the cracks to develop along the weakest zones inside the specimen and a certain part of stronger coarse aggregates are forced to damage, as well as the lateral inertial confinement effects, but cannot simulate the contributions owing to the viscosity and the strain rate effects on cement and aggregate material. Therefore the simulated strength is slightly smaller than the test result, and the difference is strain rate dependent. However, since the primary objective of the present study is to investigate the influence of pressure confinement on dynamic concrete strength, and it is difficult to accurately define the DIF related to only the viscosity and the other material strain rate effect, without further complicating the problem, this error is accepted in this study. In the subsequent simulations, the DIF is still assumed to be 1.0. Therefore the observed strength increment with strain rate is attributed to only the contributions from the different damage modes and lateral inertial confinement.

It should be noted that some researchers [19, 21] obtained the strain rate effect of concrete successfully using mesoscale concrete model in numerical simulation, implying the observed strength enhancement in impact tests is caused purely by the different damage modes of concrete material and lateral inertial confinement. These conclusions are different from the present results. As discussed above, it is commonly understood that viscosity is an important factor that contributes to the concrete material strength increment at high strain rate [2, 32]. Some testing results also demonstrate that dried concrete shows less strength increment than the wet concrete specimen [35, 37]. No mesoscale model in literature has considered the porosity and the trapped air and/or water in the concrete specimen yet owing to modelling difficulties. As shown in **Fig. 5**, neglecting these factors in mesoscale model leads to underestimation of DIF of concrete.

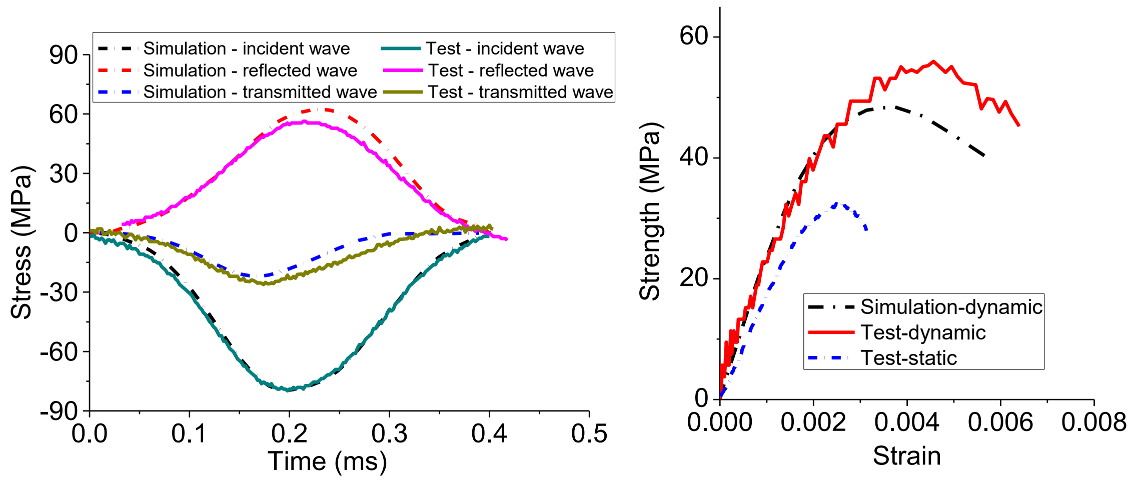

(a) (b)

Fig. 5 Comparison between the SHPB simulation results and test results: (a) stress histories; (b) stress-strain curve.

Fig. 6 shows the different failure modes of concrete under high rate loadings and low rate loadings observed in the laboratory test. It is obvious that under high-speed impact, some aggregates are cleaved, which result in more extensive cracks and hence contribute to the concrete strength increment. This does not occur when the specimen is subjected to the low-speed impact, where concrete specimen breaks into a few large fragments along the weak sections, i.e., interfaces between mortar and aggregates. This phenomenon is also captured in numerical simulations. Under low strain rate (0.1 1/s), the cracks develop along the weak sections of the concrete, i.e. the zones of mortar and aggregates interface or mortar in between aggregates, which is the brittle and stress concentrated zone in the concrete matrix. Almost no aggregate damage is observed because aggregates have higher strength than mortar matrix. Under high strain rate (65 1/s), the damage zone is more evenly distributed inside the concrete, where the mortar is damaged seriously and some aggregates are also damaged. These phenomena demonstrate the mesoscale model can reflect the strain rate effect related to the different damage modes owing to the material heterogeneity.

(a) Strain rate 65 1/s (b) Strain rate 0.1 1/s

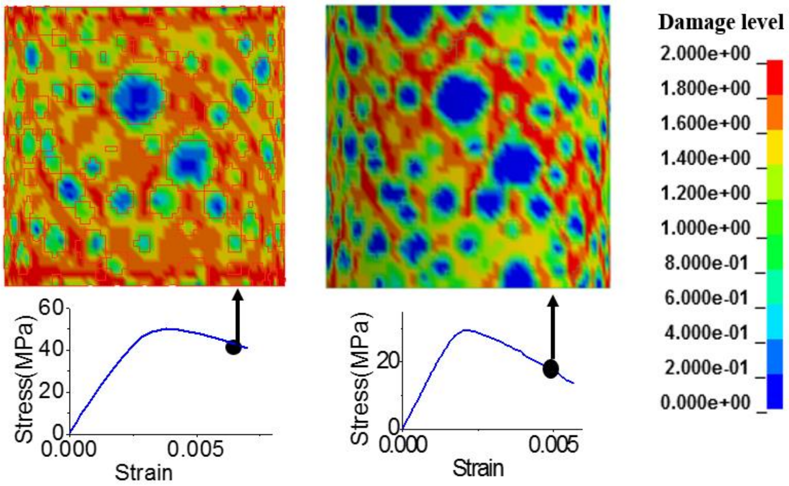

(c) Strain rate 65 1/s (d) Strain rate 0.1 1/s

Fig. 6 Failure modes of concrete under high strain rate and low strain rate loadings: (a) tested specimen at strain rate 65 1/s; (b) tested specimen at strain rate 0.1 1/s; (c) numerical result at strain rate 65 1/s; (d) numerical result at strain rate 0.1 1/s

As discussed above, the lateral inertial confinement also contributes to the strength increment. However, this contribution is relatively small (less than 10% of the static strength of the specimen) when the strain rate is lower than 100 1/s according to the study of Hao et al. [33] and Johnson and Li [38]. Nonetheless the lateral inertial confinement effect on strength increment is naturally included in the numerical simulations.

The above discussions are based on results at two strain rates only, respectively representing low and high strain rate. It should be noted that the strain rate effects are strain rate dependent, and in general become more pronounced with the increase in strain rate. In other words, the effects related to the failure modes, lateral inertial confinement, and viscosity, etc. all vary with strain rate. Nevertheless the general trend is the same as observed and discussed above. For brevity, therefore, only the results at the two strain rates are presented above to verify the numerical model and discuss the contribution factors to DIF. However, in the subsequent sections, results at more strain rates will be presented.

2.3 SHPB simulation of specimen with lateral confinement

2.3.1 Two methods of giving confinement

To simulate SHPB test with pressure confinement on specimens, a pressure vessel filled with pressurized fluid is integrated to the SHPB system to give confining pressures to the specimens, as shown in **Fig. 7**(b). This is the physical truth simulation of the laboratory tests. For comparison, as shown in **Fig. 7**(a) a constant confining pressure at the same level as that in the pressure vessel in **Fig. 7**(b) is applied on the surface of the specimen directly. In numerical simulation, a pulse load simulating the impact from the striker bar is applied to the end surface of the incident bar to load the specimens with axial loadings.

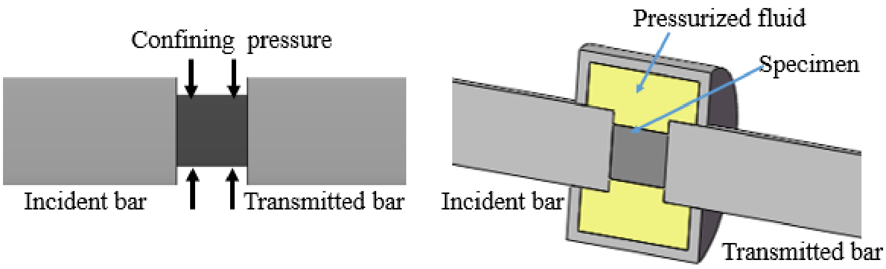

(a) model 1 (b) model 2

Fig. 7 Two models for simulation of SHPB test with confinement: (a) simplified model with a constant pressure applied on specimen surface; (b) detailed model with pressure vessel included

Two kinds of fluid, i.e., water and air are normally used for filling the pressure vessel, respectively in actual tests, and they lead to different testing results as reported by Gary and Bailly [17]. In numerical simulation in the present study, they are also considered to examine the influences of confining media on testing results. Null material and GRUNESIEN equation of state in LS-DYNA are used to simulate water pressure.

In compression, the pressure is given by,

$$p = \frac{\rho_0 C^2 \mu \left[1 + (1 - \frac{\gamma_0}{2})\mu - \frac{a}{2}\mu^2 \right]}{\left[1 - (S_1 - 1)\mu - S_2 \frac{\mu^2}{\mu + 1} - S_3 \frac{\mu^3}{(\mu + 1)^2} \right]^2} + (\gamma_0 + a\mu)E \tag{6}$$

where ρ_0 is the initial density of fluid; $\mu = \rho/\rho_0 - 1$, and ρ is the density after disturbance; C is the sound speed; γ_0 is the Gruneisen coefficient, and a is the volume correction coefficient; S_1, S_2 and S_3 are fitting coefficients; E is the specific internal energy per unit volume, the initial applied pressure is controlled by the input value of initial internal energy. These parameters are given in **Table 2** [39].

Table 2. Material parameters and coefficients in the EOS for water

Symbol	ρ_0 (kg/m^3)	C (m/s)	γ_0	a	S_1	S_2	S_3
Value	1000	1480	0.5	0	2.56	1.99	1.23

Air is modelled as an ideal gas with NULL material and LINEAR POLYNOMIAL equation of state. This EoS is given as,

$$p = C_0 + C_1 u + C_2 u^2 + C_3 u^3 + (C_4 + C_5 u + C_6 u^2)E \tag{7}$$

for ideal gas, $C_0 = C_1 = C_2 = C_3 = C_6 = 0$, $C_4 = C_5 = 0.4$ [40, 41]. The initial applied pressure is controlled by the input value of initial internal energy E; $\mu = \rho/\rho_0 - 1$, and ρ is the density after disturbance; ρ_0 is the initial density defined in the NULL material, and the density of air at the standard atmosphere pressure (0.101 MPa) is 1.225 kg/m^3. This density changes proportional to the applied pressure.

In the simulation, the inner diameter and length of the vessel are 150 mm and 100 mm, respectively. The thickness of the vessel is 10.0 mm. Lagrange solid elements of 2.0 mm cube are used to model the steel of pressure vessel with elastic material property (*Mat 1 in LSDYNA), and 2.0 mm cubic ALE solid elements are used to model the water/air which are proven yielding reliable predictions through mesh convergence tests. *CONSTRAINED_ LAGRANGE _IN_ SOLID card is coded to produce the interaction between the water/air and the solids (the specimen and the steel pressure vessel). Without loss of generality, the end friction is set to zero in the simulation of this part. Other model information is the same as described in the above section 2.2.

2.3.2 Simulation results

Two cases of confining pressures, namely 2.0 MPa and 10.0 MPa are considered in the simulation. Different loading rates in simulations are achieved by changing the amplitude of the incident sine wave. **Fig. 8** shows the peak lateral stress distribution along the radial direction of the two models when the confining pressure is 2.0 MPa and strain rate is about 120 1/s. Position 0 mm corresponds to the center of the specimen, and the position 25 mm corresponds to the free surface. It can be found that the lateral stresses of the three models differ significantly. For model 1 with direct application of the confining pressure on the specimen, the lateral stress increases to about 13 MPa at the center of the specimen during impact which is resulted due to the inertial effect caused by the Poisson's ratio. For model 2 where the same confining pressure is applied with pressurized water, the lateral stress at the surface of specimen goes beyond 10.0 MPa while at the center of specimen is over 20 MPa. It is clear that the use of vessel to apply pressurized water on the specimens leads to the increase in the confinement pressure during the test. This is because the water is almost incompressible, together with the pressure vessel they confine the lateral deformation of the specimen subjected to the axial impact. Lateral expansion of the specimen will lead to the increase of confinement pressure. For model 2 with pressurized air, the confinement pressure also increases but at a less scale than the case using pressurized water during the dynamic test because air is easier to be compressed and it has a lower density than water. These results explain the observations reported by Gary and Bailly [17] that using pressured water and air in modified SHPB tests yields different testing data. They also demonstrate that the confinement pressure changes during the impact tests owing to the specimen deformation and is substantially higher than the specified value, therefore it makes accurate interpretation of the testing results difficult because it is confinement pressure dependent but the variation in confinement pressure is basically uncontrollable.

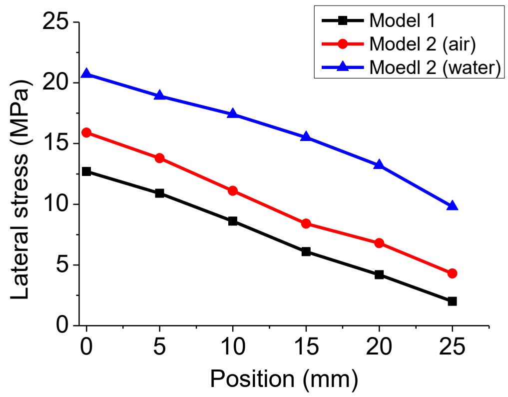

Fig. 8 Lateral stresses distribution of the two models (strain rate 120 1/s, initial confinement pressure 2.0 MPa)

To further investigate the influence of the current technique of using pressurized vessel in providing confinement pressure in modified SHPB tests on testing data, more simulations are carried out. **Fig. 9**(a) gives the strength of the concrete at different strain rates with 2.0 MPa initial confining pressure. As shown the strength of concrete from model 1 increases from 54 MPa to 74 MPa as the strain rate increases from 55 1/s to 350 1/s. Compared with that of model 1, the strength of concrete from model 2 with pressurized water increases from 65 MPa at strain rate 45 1/s to 128 MPa at strain rate 320 1/s. The similar trend can be observed for the case with pressurized air, and the results are in between the above two cases. These results indicate that the testing apparatus significantly influences the testing data of dynamic concrete strength. This is because the applied confinement pressure increases with the lateral deformation of the specimen, which provides significantly higher confinement to the concrete specimen. Therefore, the observed increase in concrete strength is not the true strain rate effect of material under a constant confining pressure of 2.0 MPa, but a varying and higher confining pressure. These results demonstrate that the current testing technique over predicts the strain rate effect on concrete strength under confinement pressure, and the level of over prediction increases with the strain rate. Using pressurized air to provide confinement gives better testing results than using pressurized water because air is more compressible and has smaller density than water. Therefore the increase in confining pressure in air is less prominent than that in water. **Fig. 9**(b) gives simulation results with 10.0 MPa initial confining pressure. Similar observations to those in **Fig. 9**(a) can be obtained. However, it can be noted by comparing the curves in **Fig. 9**(a) and **Fig. 9**(b) that the rate of strength increment with the strain rate is less prominent when the initial confinement pressure is higher. This is because the pressure increment with specimen deformation with respect to a larger initial confinement pressure is less prominent.

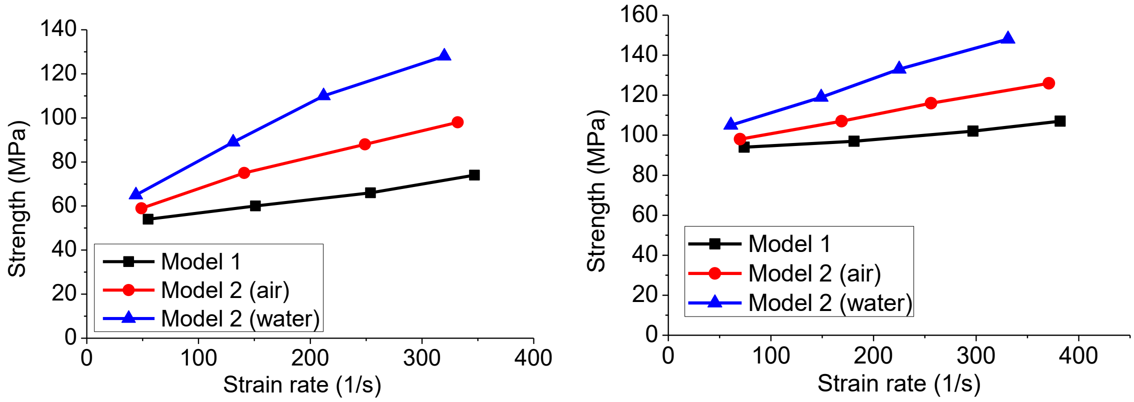

(a) (b)

Fig. 9 Strength of confined concrete at different strain rate: (a) 2.0 MPa confining pressure; (b) 10.0 MPa confining pressure

To quantify the DIF of confined concrete material in the modified SHPB test system with a pressure vessel, the corresponding DIFs obtained by the ratio of the dynamic strength of the concrete from the above model 1 and model 2 to the static strength of concrete with the same confining pressure is shown in **Fig. 10**. The unconfined strength of concrete used in the simulation is 31.7 MPa, it has a strength of 44 MPa under 2 MPa confining pressure and a strength of 85 MPa under 10 MPa confining pressure (at strain rate 0.1 1/s). It is clear that the interaction between the water/air and specimens significantly influences the pseudo tri-axial dynamic test results, and greatly over predicts the dynamic strength of confined concrete material. Since the concrete properties under tri-axial dynamic loadings is very important for establishing the dynamic concrete constitutive model, accurately obtain the true dynamic properties of confined concrete is essential. Modified testing devices with ability of properly controlling the confining pressure is deemed necessary.

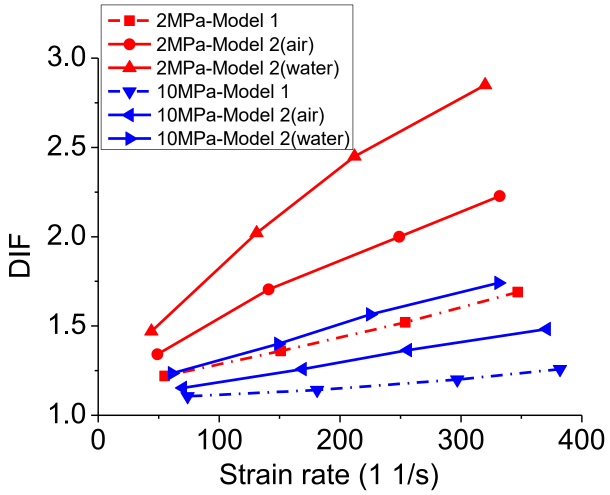

Fig. 10 DIF of confined concrete at different strain rate

3. Study of strain rate effect on confined concrete material

The above numerical results demonstrate that the current apparatus used in modified SHPB tests on confined concrete specimens do not give accurate results because confinement pressure changes with the specimen deformation. In general the current test technique over predicts the dynamic strength of confined concrete. To better understand the strain rate effect on concrete material with confinement, the mesoscale model of concrete is used to numerically simulate the modified SHPB tests of confined concrete specimens.

3.1 Numerical simulations

Three levels of confining pressures (5.0 MPa, 10.0 MPa and 15.0 MPa) are considered with the model 1 shown in **Fig. 7** to investigate their different effects on the DIF of concrete. End friction is set to zero in this study in order to concentrate on investigating the confinement effect on dynamic strength of concrete.

Fig. 11 shows the failure modes of concrete specimens under low strain rate with or without confinement, as well as the specimen without confinement under high strain rate. As shown under low rate (0.1 1/s) uniaxial impact loading, the cracks in the unconfined specimen develop along the weak sections of the concrete. Under high rate (190 1/s) uniaxial impact loading, the damage zone of the unconfined specimen is widely distributed inside the specimen with damages also occurring to aggregates. Under low strain rate (0.1 1/s) impact on specimen with 15.0 MPa confining pressure, the damage pattern is very similar to the case of unconfined specimen subjected to high rate impact, i.e., the damages also widely distribute inside the concrete specimen with damages occurring to aggregates. These observations indicate that confinement pressure and high strain rate have similar effects on the damage modes of concrete specimen. This is because the confining pressure constrains the lateral expansion of the specimen under axial impact, similar to the lateral inertial confinement, and constrains the development of large cracks hence resulting in widely distributed cracks in the specimen with many small fragments, similar to the damage mode of the specimen under high-speed impact.

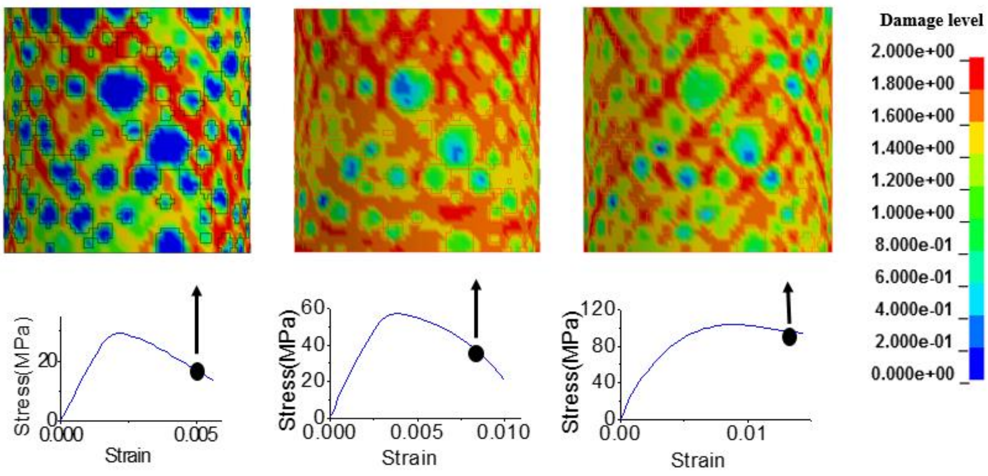

(a) (b) (c)

Fig. 11 Failure modes of concrete specimen: (a) low strain rate (0.1 1/s) without confinement; (b) high strain rate (190 1/s) without confinement; (c) low strain rate (0.1 1/s) with 15.0 MPa confining pressure

Some published experimental results also show the same phenomenon of change of the damage modes with the increment of the strain rate [22, 23]. In the experimental study by Chen et al. [22] (as shown in **Fig. 12**), the cracks passed through the mortar and propagated along a main interface under low strain rate. Under high strain rates, the stress increased so rapidly that before the crack had time to extend along the path of least resistance, the stress had increased to sufficient level to fracture the mortar zones and aggregates of higher strength.

In the study of reference [11] as shown in **Fig. 13** that under static unconfined uniaxial loadings, the concrete specimen failed with a dominant crack penetrating through the entire specimen. When the applied confining pressure was high, the confinement restricted the cracks to develop along the original weakest zone in the concrete and more intensive damage to cement matrix and aggregates was created, which therefore led to more damage surfaces and hence more number of smaller fragments. These results show that the damage modes of concrete specimens under uniaxial high-speed impact and static load with confinement are somewhat similar, implying again the strain rate and lateral pressure confinement effects are similar on concrete material properties.

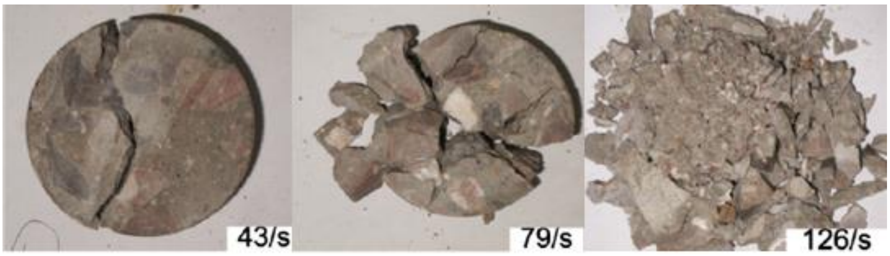

Fig. 12. Failure mode of unconfined concrete specimens under different strain rates [22].

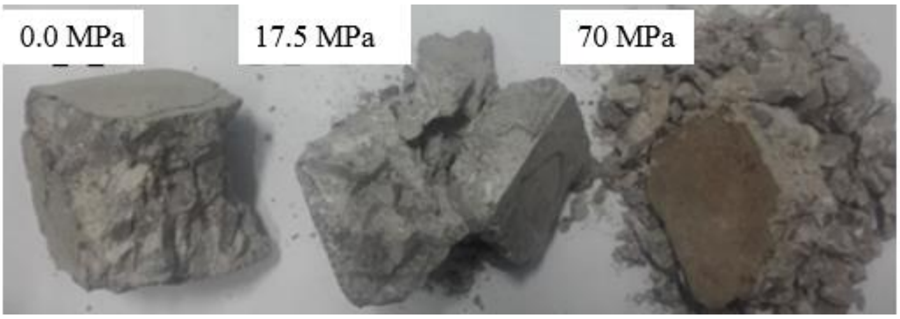

Fig. 13. Failure mode of concrete specimens under static tests with different confining pressures [11]

Fig. 14 shows the strain rate effect on mesoscale model of concrete with and without confinement on specimens. Because the concrete material DIF is assumed to be 1.0 in the simulation, for the case of unconfined specimen under uniaxial loading, the obtained strength increment can be attributed to the strain rate effect related to the different failure modes and the lateral inertial confinement (structural effect) as discussed above. It can be seen from **Fig. 14 (a)**, under a strain rate of 187 1/s, the dynamic strength of concrete increases about 80% compared to its strength at strain rate 0.1 1/s. Because the strength increment caused by the lateral inertial confinement is less than 20% of the concrete static strength when the strain rate is lower than 200 1/s [33, 38], the observed strength increment can therefore be primarily attributed to the changing damage modes at high strain rates. However as shown in **Fig. 14 (b)**, when a 15.0 MPa confining pressure is applied to the specimen, the simulated stress-strain curve of the specimen at the same two strain rates are similar, indicating the strain rate effect is insignificant. These results show that under this level of confining pressure, the concrete material properties are not significantly influenced by the strain rate effect associated to the changing in damage mode.

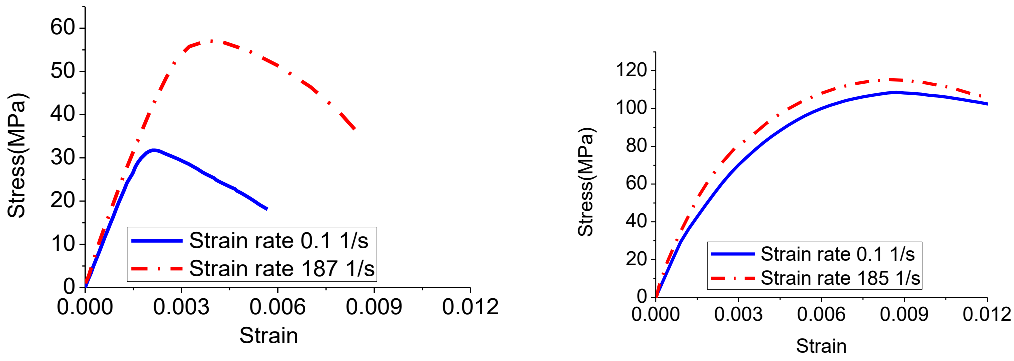

(a) (b)

Fig. 14 Strain rate effect of meso-scale concrete model: (a) no confinement; (b) 15 MPa confining pressure.

More simulations are carried out with different level of confining pressures at different strain rates. The detail results are not shown here for brevity. It is found that the strain rate effects on concrete compressive strength are confining pressure dependent. Based on the simulation results, an empirical relation of DIF of concrete as a function of confining pressure p_c, denoted as DIF_{pc}, is defined as:

$$\mathrm{DIF}_{pc}=r\,(p_c)\,(\mathrm{DIF}_0-1)+1 \tag{8a}$$

or

$$r\,(p_c)=(\mathrm{DIF}_{pc}-1)\,/\,(\mathrm{DIF}_0-1) \tag{8b}$$

where DIF_0 is the DIF of concrete when the confining pressure is zero, $r\,(p_c)$ is the reduction factor of DIF of concrete with a confining pressure p_c. The simulation results of $r\,(p_c)$ are given in **Table 3** and **Fig. 15**. The results clearly show that DIF decreases with the increment of the confining pressure. It should be noted that the confining pressure p_c is a constant in the numerical simulation, which, as demonstrated above, is not likely to be kept constant with the current testing apparatus.

Table 3 Simulation results of strain rate effect under confining pressures

Confining pressure (MPa)	0			5			10			15		
Strain rate (1/s)	0.1	90	190	0.1	90	190	0.1	90	190	0.1	90	190
Strength of concrete (MPa)	31.7	50.1	57.0	59.5	75.2	79.2	85.0	94.7	97.4	108.6	112.4	114.9
DIF_{pc}	\	1.58	1.79	\	1.27	1.33	\	1.12	1.15	\	1.03	1.06
$r\,(p_c)$	\	\	\	\	0.47	0.42	\	0.21	0.19	\	0.05	0.08

In **Fig. 15**, the horizontal coordinate is the nominal confining pressure p_c*, defined as the ratio of the confining pressure to the uniaxial compressive strength of concrete. The fitted curve shown in figure is:

$$r\,(p_c^*) = \exp\,(-\,5.0\,p_c^*) \quad R^2=0.96 \tag{9}$$

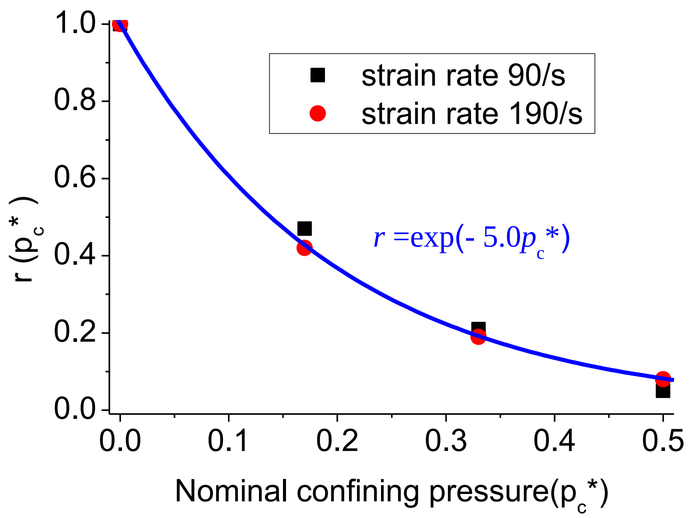

Fig. 15 The reduction of DIF under confining pressures

3.2 Modification of DIF used in the concrete model

Fig. 15 demonstrates that the DIF of the concrete decreases with the increment of the confining pressure at the same strain rate, therefore the DIF of concrete should be correlated to the stress state in the dynamic material constitutive model. Using DIF from uniaxial testing results to consider the strain rate effect of concrete properties under multi-axial compressive stress states overestimates the concrete strength.

In the concrete model, the strength of concrete is defined using equivalent stress at failure as function of pressure [30]. **Eqs. (10)-(11)** give the expressions of equivalent stress σ_{eq} and pressure p, respectively.

$$\sigma_{\mathrm{eq}}=\sqrt{\frac{1}{2}\left[(\sigma_1-\sigma_2)^2+(\sigma_2-\sigma_3)^2+(\sigma_1-\sigma_3)^2\right]} \tag{10}$$

$$p=\frac{1}{3}\left(\sigma_1+\sigma_2+\sigma_3\right) \tag{11}$$

where σ_1, σ_2 and σ_3 are the three principle stresses ($\sigma_1 \geq \sigma_2 \geq \sigma_3 \geq 0$ in this study). Therefore establishment of the DIF correlated to pressure is a convenient way to deal with the strain rate effect under multi-axial stress states in the concrete model. In the case of uniaxial compression, σ_1 is the uniaxial strength of concrete f_c, $\sigma_2 = \sigma_3 = 0$, thus $p = 1/3\ f_c$. Therefore the failure of concrete under a pressure lower than $1/3\ f_c$ occurs due to the combined tensile and compressive stress states or multi-axial tensile stress states. The modifications of DIFs in these stress states are beyond the scope of the present study because of lack of corresponding data. When $p > 1/3\ f_c$, i.e., the material is under multi-axial compressive stress, instead of using the DIF derived from uniaxial testing data, it is suggested to model the DIF according to the simulation results given in **Table 3**. **Fig. 16** shows the reduction factor of DIF as function of nominal pressure p^*, defined as the ratio of the pressure p to the uniaxial compressive strength of concrete f_c. In the current cases, $\sigma_2 = \sigma_3$ is the cylindrical symmetric confining pressure p_c, σ_1 is the static strength of concrete with confinement pressure p_c, then $p^* = (\sigma_1 + 2\ p_c) / (3f_c)$. The best fitted curve as shown in **Fig. 16** can be expressed by **Eq. (12)**

$$r(p^*)=\begin{cases}1 & p^*\leq\dfrac{1}{3} \\ \exp[-2.1(p^*-\dfrac{1}{3})] & p^*>\dfrac{1}{3} \qquad R^2=0.94\end{cases} \tag{12}$$

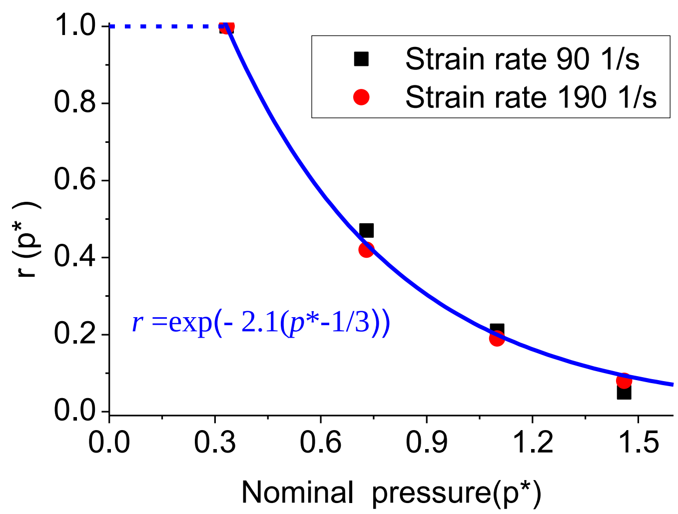

Fig. 16 The reduction of DIF corresponding to the pressures

Therefore, the uniaxial dynamic increase factor DIF is correlated to pressure by,

$$\mathrm{DIF}(p^*) = r\,(p^*)\,(\mathrm{DIF} - 1) + 1 \tag{13}$$

It should be noted that the contribution of viscosity and other factors to the strain rate effect under complex stress states is still unaware. Strain rate effects under multi-axial stress states are extremely complex and more intensive studies should be carried out. Developing reliable tri-axial dynamic test devices is the best way to study the concrete properties under dynamic multi-axial stress states. The above proposed empirical formula can be used to approximately model the concrete material DIF under multi-axial stress states, which provides more accurate predictions of concrete materials at high strain rates.

4. Conclusion

This paper built a mesoscale model of concrete specimen to simulate SHPB tests. The accuracy of the model was verified with testing data. Intensive numerical simulations of SHPB tests of concrete specimens without or with lateral pressure confinement at different strain rates were carried out. The numerical results demonstrated that the current modified SHPB test technique with pressure confinement on concrete specimen over predicted the concrete dynamic strength because the confinement pressure would increase with the specimen deformation under high-speed impacts. Pressure vessel filled with pressurized water used in the modified SHPB tests led to more significant over prediction of dynamic concrete strength than that filled with pressurized air because water is less compressive and has higher density than air. The results provided explanations on experimental observations that SHPB tests on specimens with pressure confinement led to different results if the confinement medium was different. It was also found and explained that under lateral pressure confinement the concrete material was less strain rate sensitive as compared to the specimens tested without confinement because the high-rate impact and pressure confinement led to the similar failure mode of concrete specimens and pressure confinement also reduced the lateral inertial confinement effect. Based on the numerical simulation results, an empirical relation was proposed to modify the unconfined concrete strength DIF obtained from uniaxial impact tests for concrete material with pressure confinement. The proposed empirical formula can be used to more accurately model the dynamic strength increment of concrete material under pressure confinement.

5. Acknowledgments

The authors gratefully acknowledge the support from China National Nature Science Foundation under grant number 51378346, and Australian Research Council under grant number DP160104557 for carrying out this research.

6. References

[1] Yan D, Lin G, Chen G. Dynamic properties of concrete under multi-axial loading. In: Advance in Materials Scinece Research. 2011;1:145-82.

[2] Cui J, Hao H, Shi Y. Discussion on the suitability of concrete constitutive models for high-rate response predictions of RC structures. International Journal of Impact Engineering. 2017;106:202-16.

[3] Bischoff P, Perry S. Compressive behaviour of concrete at high strain rates. Materials and structures. 1991;24:425-50.

[4] Grote D, Park S, Zhou M. Dynamic behavior of concrete at high strain rates and pressures: I. experimental characterization. International journal of impact engineering. 2001;25:869-86.

[5] Hao Y, Hao H, Zhang X. Numerical analysis of concrete material properties at high strain rate under direct tension. International Journal of Impact Engineering. 2012;39:51-62.

[6] Hao Y, Hao H. Finite element modelling of mesoscale concrete material in dynamic splitting test. Advances in Structural Engineering. 2016;19:1027-39.

[7] Du Béton FI. fib model code for concrete structures 2010. Berlin, Germany. 2013.

[8] Candappa D, Sanjayan J, Setunge S. Complete triaxial stress-strain curves of high-strength concrete. Journal of Materials in Civil Engineering. 2001;13:209-15.

[9] Sfer D, Carol I, Gettu R, Etse G. Study of the behavior of concrete under triaxial compression. Journal of Engineering Mechanics. 2002;128:156-63.

[10] Vu XH, Malecot Y, Daudeville L, Buzaud E. Experimental analysis of concrete behavior under high confinement: Effect of the saturation ratio. International Journal of Solids and Structures. 2009;46:1105-20.

[11] Cui J, Hao H, Shi Y, Li X, Du K. Experimental study of concrete damage under high hydrostatic pressure. Cement and Concrete Research. 2017;100:140-52.

[12] Yan D, Lin G, Chen G. Dynamic properties of plain concrete in triaxial stress state. Materials journal. 2009;106:89-94.

[13] Fujikake K, Mori K, Uebayashi K, Ohno T, Mizuncr J. Dynamic properties of concrete materials with high rates of tri-axial compressive loads. WIT Transactions on The Built Environment. 2000;48.

[14] Chen J, Zhang Z, Dong H, Zhu J. Experimental study on dynamic damage evolution of concrete under multi-axial stresses. Engineering Failure Analysis. 2011;18:1784-90.

[15] Xue Z, Hu S. Dynamic behavior of cement mortar under active confinement Explosion and Shock Waves (in Chinese). 2008;6:561-4.

[16] Malvern LE, Jenkins D. Dynamic testing of laterally confined concrete. California inst of tech pasadena dept of information sciences; 1990.

[17] Gary G, Bailly P. Behaviour of quasi-brittle material at high strain rate. Experiment and modelling. European Journal of Mechanics-A/Solids. 1998;17:403-20.

[18] Malvar LJ, Simons D. Concrete material modeling in explicit computations. Workshop on recent advances in computational structural dynamics and high performance computing: USAE Waterways Experiment Station; 1996. p. 165-94.

[19] Huang Y, Yang Z, Chen X, Liu G. Monte Carlo simulations of meso-scale dynamic compressive behavior of concrete based on X-ray computed tomography images. International Journal of Impact Engineering. 2016;97:102-15.

[20] Chen G, Hao Y, Hao H. 3D meso-scale modelling of concrete material in spall tests. Materials and Structures. 2015;48:1887.

[21] Zhou R, Song Z, Lu Y. 3D mesoscale finite element modelling of concrete. Computers & Structures. 2017;192:96-113.

[22] Chen X, Wu S, Zhou J. Experimental and modeling study of dynamic mechanical properties of cement paste, mortar and concrete. Construction and Building Materials. 2013;47:419-30.

[23] Fu Q, Xie Y, Long G, Niu D, Song H, Liu X. Impact characterization and modelling of cement and asphalt mortar based on SHPB experiments. International Journal of Impact Engineering. 2017;106:44-52.

[24] Lu Y, Chen X, Teng X, Zhang S. Dynamic compressive behavior of recycled aggregate concrete based on split Hopkinson pressure bar tests. Latin American Journal of Solids and Structures. 2014;11:131-41.

[25] Xiao J, Li L, Shen L, Poon CS. Compressive behaviour of recycled aggregate concrete under impact loading. Cement and Concrete Research. 2015;71:46-55.

[26] Yan D, Lin G. Influence of initial static stress on the dynamic properties of concrete. Cement and Concrete Composites. 2008;30:327-33.

[27] Zhou X, Hao H. Modelling of compressive behaviour of concrete-like materials at high strain rate. International Journal of Solids and Structures. 2008;45:4648-61.

[28] Davies E, Hunter S. The dynamic compression testing of solids by the method of the split Hopkinson pressure bar. Journal of the Mechanics and Physics of Solids. 1963;11:155-79.

[29] Cui J, Hao H, Shi Y. Study of concrete damage mechanism under hydrostatic pressure by numerical simulations. Construction and Building Materials (under review). 2017.

[30] Malvar LJ, Crawford JE, Wesevich JW, Simons D. A plasticity concrete material model for DYNA3D. International Journal of Impact Engineering. 1997;19:847-73.

[31] Software LSDYNA. Livermore Software Technology Corporation. Livermore, CA.

[32] Hao H, Hao Y, Li J, Chen W. Review of the current practices in blast-resistant analysis and design of concrete structures. Advances in Structural Engineering. 2016;19:1193-223.

[33] Hao Y, Hao H, Li Z-X. Numerical analysis of lateral inertial confinement effects on impact test of concrete compressive material properties. International Journal of Protective Structures. 2010;1:145-67.

[34] Zhang M, Wu H, Li Q, Huang F. Further investigation on the dynamic compressive strength enhancement of concrete-like materials based on split Hopkinson pressure bar tests. Part I: Experiments. International journal of impact engineering. 2009;36:1327-34.

[35] Ross CA, Jerome DM, Tedesco JW, Hughes ML. Moisture and strain rate effects on concrete strength. Materials Journal. 1996;93:293-300.

[36] Hao Y, Hao H. Numerical evaluation of the influence of aggregates on concrete compressive strength at high strain rate. International journal of protective structures. 2011;2:177-206.

[37] Rossi P. Influence of cracking in the presence of free water on the mechanical behaviour of concrete. Magazine of concrete research. 1991;43:53-7.

[38] Flores-Johnson E, Li Q. Structural effects on compressive strength enhancement of concrete-like materials in a split Hopkinson pressure bar test. International Journal of Impact Engineering. 2017;109:408-18.

[39] Liu M, Liu G, Lam K. Investigations into water mitigation using a meshless particle method. Shock waves. 2002;12:181-95.

[40] Alia A, Souli M. High explosive simulation using multi-material formulations. Applied thermal engineering. 2006;26:1032-42.

[41] Cui J, Shi Y, Li Z-X, Chen L. Failure Analysis and Damage Assessment of RC Columns under Close-In Explosions. Journal of Performance of Constructed Facilities. 2015; 29: B4015003.